

5A096-2665C

CONF-97015--1

THERMALLY INDUCED EVOLUTION OF MORPHOLOGY ON CERAMIC SURFACES IN A THERMIONIC CONVERTER

Kevin R. Zavadil
Sandia National Laboratories
P.O. Box 5800
Albuquerque, NM 87185-0342
505-845-8442

David L. Olson
Team Specialty Services
901 University Blvd. SE
Albuquerque, NM 87106-4439
505-272-7266

Alexander E. Klinkov
JS INTERTEK
123182 Moscow
Kurchatov Sq. 1

Abstract

The morphology of alumina and scandia ceramics exposed to controlled vacuum and diffusion modes in a thermionic converter has been studied. Evidence for vaporization at a temperature of 1770 K is manifest in the resulting surface morphologies of both ceramics, consistent with reported sample mass loss. Alumina shows intergranular relief with the formation of terrace - step structure on the grain surfaces. Terrace formation is not directly observed on scandia, however the development of vertical structure and maintenance of voids indicates that vaporization is initiated by structure at the grain edges. Extensive Sc_2O_3 re-deposition occurs on the scandia surface, possibly mediated by the presence of molybdenum and tungsten. Evidence exists for refractory metal secondary phase formation in this deposit in the form of $\text{Sc}_6\text{MO}_{12}$ ($M = \text{W}$ or Mo). Alumina also shows evidence for materials' interactions in the form of tantalum assisted vaporization which significantly alters the terrace structure.

INTRODUCTION

Ceramic materials are often used as mechanical spacers in the interelectrode gap of thermionic conversion devices. Scandia (Sc_2O_3) has been the material of choice for the TOPAZ-II thermionic fuel elements. The spacer's primary function is to maintain a critical gap distance at operational temperatures when emitter distortion occurs. These materials are immersed in a Cs plasma and are subjected to a host of energetic, thermal and mechanical stresses. Degradation of these materials can directly impact both the performance and longevity characteristics of a converter. Variations in the mechanical stability of metal oxide insulators can lead to changes in interelectrode gap distances and changes in converter efficiency. Material loss from the spacer through vaporization reactions (Kozlov et al. 1993) will lead to shifts in the interelectrode material balance and possibly changes in the plasma characteristics. As a result, the chemical and physical roles these material play need to be understood.

In this paper, we report on the morphology of scandia and alumina surfaces subjected to vacuum and diffusion mode exposure. The vacuum and diffusion modes for a converter are defined as operation at the operational emitter temperature with the interelectrode gap evacuated or pressurized with cesium, respectively (Baksht et al. 1978). These two modes are the precursors to the ignited mode where electron flux is allowed from emitter to collector. These two modes represent the first step in understanding what processes are expected to take place on the spacer surfaces. Kozlov et al. (1995) have shown that vaporization of both alumina and scandia occur at 1770 K for these two modes. The gravimetrically determined vaporization rates show a trend of an approximate 10-fold decrease on passing from vacuum to diffusion modes (7×10^{-9} to 8×10^{-10} and 6×10^{-10} to 7×10^{-11} $\text{kg/m}^2\text{sec}$) for both alumina and scandia. Ignited mode operation produces an increase in evaporation rate (5-fold relative to the vacuum mode) as well as large-scale microstructural changes for alumina, while scandia shows no discernible change in vaporization rate or microstructure (Kozlov et al. 1995). We have conducted an analogous set of experiments and report on the resulting microstructural evolution. Vaporization from most oxides results in the dissociative formation of the metal species and substoichiometric oxides (Lamoreaux et al. 1987). These processes represent reactions that can be chemically assisted. Our goal is to use this microstructural information, as well as some surface compositional information, to better understand these vaporization reactions within a converter environment. Attempts to identify stable ceramic materials for this application will require an understanding of how microstructure and composition impact these reactions.

MASTER DISTRIBUTION OF THIS DOCUMENT IS UNLIMITED

DISCLAIMER

This report was prepared as an account of work sponsored by an agency of the United States Government. Neither the United States Government nor any agency thereof, nor any of their employees, makes any warranty, express or implied, or assumes any legal liability or responsibility for the accuracy, completeness, or usefulness of any information, apparatus, product, or process disclosed, or represents that its use would not infringe privately owned rights. Reference herein to any specific commercial product, process, or service by trade name, trademark, manufacturer, or otherwise does not necessarily constitute or imply its endorsement, recommendation, or favoring by the United States Government or any agency thereof. The views and opinions of authors expressed herein do not necessarily state or reflect those of the United States Government or any agency thereof.

DISCLAIMER

**Portions of this document may be illegible
in electronic image products. Images are
produced from the best available original
document.**

EXPERIMENTAL

The test system used for conducting controlled exposures of the ceramics samples has been previously described by Kozlov et al. (1995). Four alumina and two scandia test samples were acquired from RI of SIA. Initial microstructure and purity were examined to characterize these materials prior to testing (Kozlov et al. 1995). The samples are partially bored cylinders (for thermocouple insertion) with an optical flat ground and polished along the sample length. All microstructural and compositional characterization were conducted at various points along this surface. These six samples were first subjected to 300 hours of vacuum mode exposure followed by 400 hours of diffusion mode exposure.

Vaporization loss rates were determined gravimetrically by sample weighing before and after exposure. We calculate an average exposure temperature of 1770 ± 20 K. Due to the design of the emitter, Mo deposition occurs along the circumference of the sample, as opposed to the optical flat, and impacts these mass measurements. Post-exposure annealing to 1000°C in both air and vacuum for several hours was used to remove the Mo. Light brushing and ethanol rinsing of the samples was used to remove remaining particulate from the oxidation and sublimation of the Mo. Samples were then re-heated to fully volatilize the ethanol.

Post-exposure surface microstructure was evaluated using a combination of mechanical and micrographic techniques. Profilometry was conducted on a Dektak-IIA using a $12.5 \mu\text{m}$ stylus with a loading force of 2.5×10^{-4} N. Optical profilometry was performed using a Wyko RST Plus microscope in a phase-shifting interferometric mode. Scanning electron micrographs were generated with a Hitachi S-570 microscope using a 25 kV primary beam. An approximate 300 Å Pt or Pt/Au overlayer was used for charge neutralization. These thin films were removed by immersion of the sample in aqua regia at 60°C followed by extensive rinsing and elevated temperature drying. A JEOL JXA 8600 microprobe was used to generate semi-quantitative compositional information in both energy and wavelength dispersive modes. Near-grazing angle x-ray diffraction was performed on a Siemens D500 diffractometer using a fixed 2° incident angle, a variable detector angle and a Cu ($K\alpha$) source. We estimate a sampling of $1 \mu\text{m}$ for a fully dense scandia layer under these conditions.

RESULTS AND DISCUSSION

Thermal annealing of the alumina ceramic samples produces a number of anticipated surface microstructural changes. Figure 1 shows optical micrographs of the alumina samples prior to and after annealing in the interelectrode gap. A comparison of these micrographs shows that the average grain size has increased, based on the disappearance of the sub-micron grains prevalent in the initial sample. This form of grain enlargement or coarsening is typical for ceramic materials that are subjected to extended periods of annealing. Vaporization has occurred based on a measurable mass loss and a calculated, average vaporization rate (j) for the alumina samples, as shown in Table

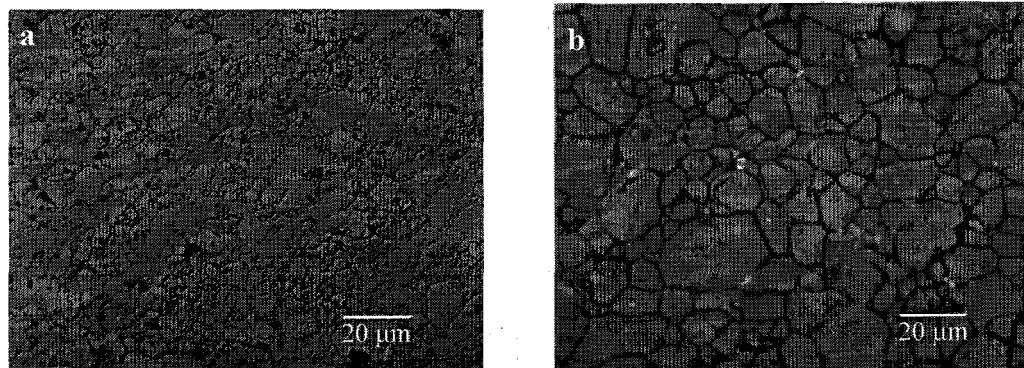


FIGURE 1. Optical Micrographs of an Alumina Sample a) before Vacuum Annealing and b) after Diffusion Mode Exposure (750X magnification).

1. We also find that a considerable degree of grain relief has occurred at the perimeter of the grains, indicating either preferential vaporization and/or mass transport from the grain boundaries. The contact profilometric data shown in Table 1 shows that most of the large scale microstructural changes observed in Figure 1 result from vacuum annealing as opposed to subsequent annealing in the presence of Cs. The average height of a surface feature (R_s) increases from 40 ± 13 nm to 242 ± 98 and 222 ± 100 nm after vacuum and diffusion mode exposure, respectively. A 10-fold increase is observed for the average slope of a surface feature (δ_a) from 4.0 ± 0.7 to 40 ± 7 mrad with annealing, with no significant change observed for subsequent annealing in the presence of Cs. The average length scale (λ_a) for a surface feature decreases by approximately a factor of two from 64 ± 25 to 37 ± 9 μm , also with no significant change observed for Cs exposure. These changes in the average height, slope and length scale for the surface features indicate that the microstructural changes are produced primarily by grain development with extended annealing, within the limit of sampling constraints due to the size and shape of the stylus. Of note, is the fact that the vaporization rate for alumina measured for the vacuum mode is a factor of 6 times greater than that determined by Kozlov et al. (1995) and we do not observe a decrease in this rate in the presence of Cs.

Table 1. Contact Profilometric and Average Vaporization Rate Values for Ceramic Test Samples

Sample & Mode	R_s (nm)	δ_a (mrad)	λ_a (μm)	j ($\text{kg}/\text{m}^2\cdot\text{sec}$)
Al_2O_3 initial	40 ± 13	4.0 ± 0.7	64 ± 25	----
Al_2O_3 vacuum	297 ± 73	43 ± 6	43 ± 8	4.2×10^{-8}
Al_2O_3 diffusion	363 ± 124	50 ± 20	46 ± 8	1.6×10^{-7}
Sc_2O_3 initial	11 ± 2	2.5 ± 0.5	28 ± 9	----
Sc_2O_3 vacuum	81 ± 6	21 ± 4	24 ± 3	2.3×10^{-8}
Sc_2O_3 diffusion	106 ± 14	22 ± 4	30 ± 2	1.3×10^{-8}

Electron microscopy shows additional evidence for sublimation related microstructural evolution on the alumina ceramics. Figure 2 shows a high resolution secondary electron image of an alumina sample after diffusion mode exposure. The image was generated using a 45° incident angle to accentuate fine surface texture. The surface of an individual grain is visible in this image. The grain face shows some undulating morphology as well as significant vertical relief between the adjacent grain face (top of image), consistent with the large scale topography found in the contact profilometry measurements. The grain also possesses a more fine scale structure at its surface. This image shows steps that run the length of the grain surface. These steps result from large scale terrace structures produced by transport of alumina from the low energy step edges and eventual vaporization (Hirth and Pound 1957). These types of structures are common and easily detected on optically flat, sapphire surfaces (Heffelfinger 1995, Peleg and Alcock 1974). The presence of this terrace-step structure, along with grain boundary relief, is the primary microstructural indication that vaporization has occurred.



FIGURE 2. Electron Micrograph of an Alumina Sample after Diffusion Mode Exposure (6000X).



FIGURE 3. Electron Micrograph of an Alumina Sample near a Ta Retaining Strap after Diffusion Mode Exposure (6000X).

Microstructural evidence exists for chemically-assisted vaporization of alumina. Figure 3 shows a select region of the alumina surface in close proximity to a Ta strap used to retain the sample against the emitter. The image shows the boundary of three grains or a triple point. Along with some deposit structure (bright features), the grain faces show the presence of fine structure that appears as platelets in a plan view (left grain). The edges of these platelets are visible on the top and right grain faces. The development of considerable vertical structure is evident along the boundary between the left and right grain faces. This region of modified surface morphology extends approximately 3 mm away from the position of the strap toward the sample center. A possible explanation for this structure is that the vaporization reaction mechanism has been significantly altered by the activity of a reagent at the surface or in the vapor phase immediately adjacent to the surface. This reagent promotes vaporization from a variety of sites and limits the distance over which a terrace propagates. This altered mechanism results in the disconnected terraces visible in Figure 3. Alteration of the respective surface diffusion coefficients that describe material movement on these terraces is one way of altering the overall mechanism (Peleg and Alcock 1974).

An indication of which reagents are responsible for this altered vaporization mechanism can be inferred by looking for a variation in the chemical composition of deposited material on the surface. The converter environment most closely approximates a condition of Langmuir or free evaporation (Paule and Margrave 1967) largely because of the lower temperature collector acting as a point of condensation. Vaporization reactants can re-deposit on the ceramic provided the condensation coefficient is appreciable and they have a less than unity probability for condensation at the collector or if they undergo interspecies collision within the gap. At 1 torr Cs pressure, the mean free path for Cs at 1770 K is approximately one third of the interelectrode gap spacing of 0.5 mm, making collisional reflection a likely process. The surface shows scattered deposits of columnar crystals like those shown in Figure 3. X-ray analysis has been used to analyze the composition of these crystals in the region showing this altered morphology as well as the remainder of the surface. Crystals within the altered morphology region contain both Ta and Nb while crystals outside of this region contain primarily Nb with no detectable Ta. These findings indicate that Ta subliming from the strap at 1770 K is responsible for the altered mechanism. Semi-quantitative wavelength dispersive x-ray analysis conducted on deposits outside of this region yield a 1:1 Al:Nb stoichiometry indicative of AlNbO_4 formation. We presume that the crystal composition within the modified region is also the niobate along with solid solutions of both aluminum and tantalum oxides (Roth and Waring 1970). Nb most likely arrives at the surface from the collector (900 K) as a substoichiometric oxide. X-ray analysis has also shown the presence of CaMoO_4 polymorphic deposits on the surface at substantially lower relative abundance and uniform distribution. Ca is most likely being released, through surface segregation, from the alumina samples (0.06 wt.%). Scandium was not detected on the alumina surfaces indicating that cross-contamination from an adjacent scandium sample, known to undergo mass loss, does not occur. We estimate our sensitivity for scandium detection to be approximately 0.1 wt.%.

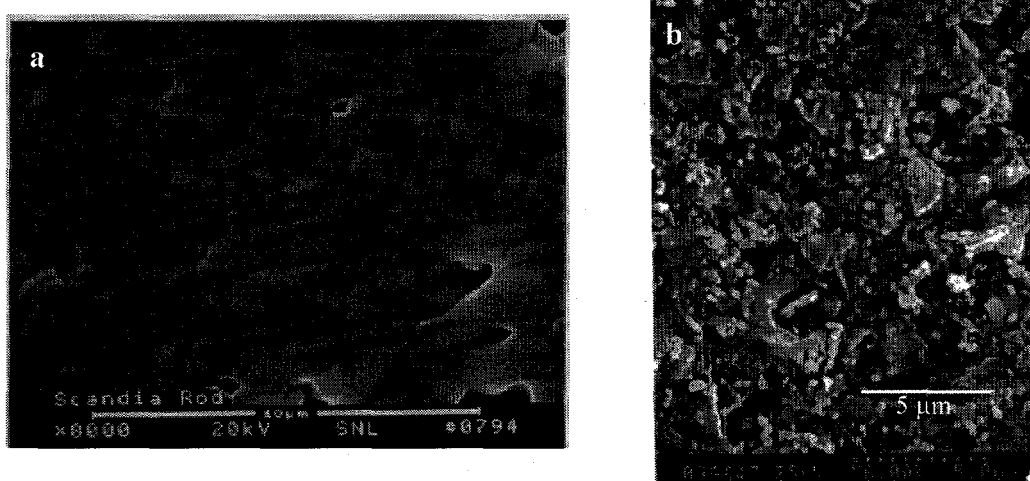


FIGURE 4. Electron Micrographs of a Scandia Sample a) before Vacuum Annealing (8000X) and b) after Diffusion Mode Exposure (6000X).

The scandia surface shows a considerably greater degree of microstructural evolution with annealing. Figure 4 shows secondary electron micrographs generated for a scandia sample prior to vacuum mode exposure and after diffusion mode exposure. A comparison of these images shows that the grain structure and voids are visible under a nucleating deposit after diffusion mode exposure. The underlying morphology appears to be independent of distance from the Ta retaining strap. Direct comparison of grain sizes before and after diffusion mode exposure is difficult due to the presence of both the deposit and the development of a considerable amount of vertical texture in the grains themselves. Despite the lack of visible terrace structure in Figure 4, this vertical texture along with the continued presence of voids argues that the grain edges supply the sites for eventual vaporization of scandia. The smaller average grain size should result in a greater degree of structural variation at the scandia surface when compared to the alumina surface. This trend can be argued based on the contact profilometric data of Table 1 where the average roughness of a surface feature has increased by an order of magnitude with no significant change in the average wavelength. The fact that scandia has undergone vaporization is evident from the calculated average vaporization rates shown in Table 1. We note that, while we do observe a decrease in rate in the presence of Cs, our values of vaporization rates are one to two orders of magnitude greater than those reported by Kozlov et al. (1995).

Large-scale deposition has occurred in select regions of the scandia surface. The optical interferogram of Figure 5 shows that islands have formed on the surface. These islands vary in shape and size. Island size can vary from several tens of microns to hundreds of microns in cross-section and three to five microns in height. Island-free regions as large as several hundred microns can separate individual islands. An electron micrograph generated from an island top is also shown in Figure 5. This image shows that the islands are comprised of a densely matted, fibril-type structure. These fibrils appear identical in shape to the deposit structures visible in Figure 4, which was generated in an island-free region. The fibrils possess sub-micron cross-sectional diameters and lengths of several microns. These fibrils are oriented in a range of directions with respect to the surface plane and form a mass that has an undulating texture, complete with troughs and voids. The micrographic and interferometric data indicate that deposition has occurred across the entire surface and specific regions exist where nucleation and growth are greatly enhanced, resulting in the formation of these islands.

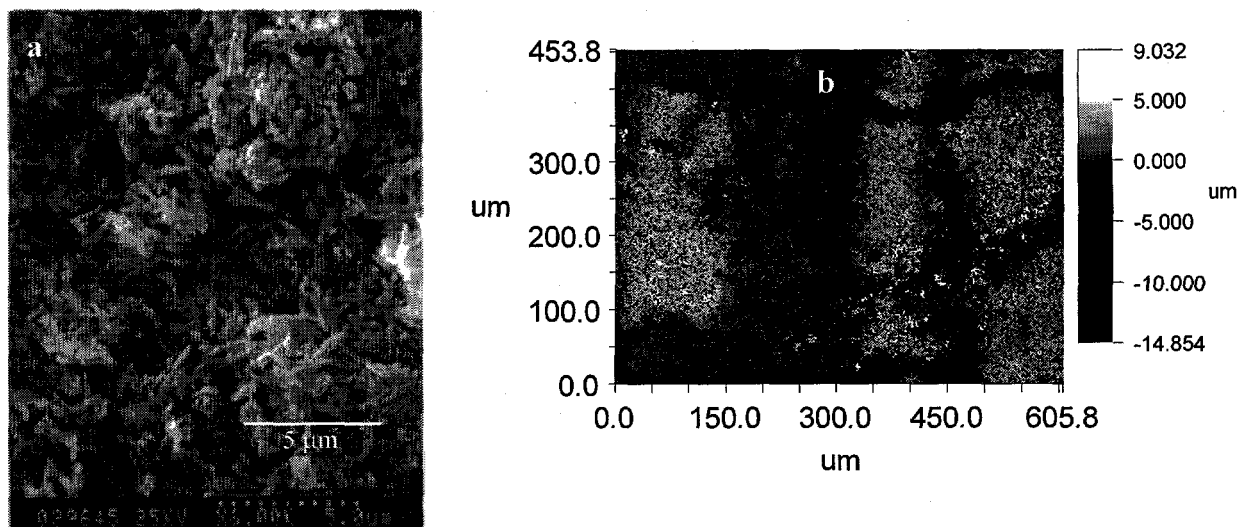


FIGURE 5. a) Electron Micrograph (6000X) and b) Optical Interferogram (10X) of the Island Deposit Morphology

This deposit is primarily scandia that contains significant concentrations of tungsten and molybdenum. Wavelength dispersive x-ray analysis shows that both of these refractory metals are present at 4 and 6 wt.%, respectively. Sampled regions off of these islands show significant decreases in refractory metal content to levels below 0.2 wt.%. These trends indicate that W and Mo are predominantly, but not exclusively, associated with the islands. Given the varying density of newly nucleating material observed in electron microscopy, a reduced signal

from W and Mo would be expected even on the island-free regions of the surface. A several-fold variation in relative concentration between W and Mo is also observed indicating that the island composition of these metals is not fixed. X-ray fluorescence does not show the presence of Al in these islands, ruling out the possibility that they result from the transport of material from adjacent eroding alumina samples.

The presence of tungsten and molybdenum in the re-deposited scandia suggests that a chemical interaction may drive this re-deposition process. Based on the concentrations determined by x-ray analysis, we would expect a molar ratio of Sc:W:Mo of between 98:2:6 which indicates that the refractory metals must be present in a minority phase. Grazing angle x-ray diffraction was conducted to identify the presence of crystalline product phases in the deposit. Two areas were imaged on a scandia sample - one of high and one of low island abundance. We calculate a 1.25 μm sampling depth at a 2° incident angle for fully dense Sc_2O_3 , indicating a reasonable degree of specificity for these islands given their average height. Both regions showed predominate Sc_2O_3 features, however, a series of six features not expected for scandia were found to increase in relative intensity with increasing island abundance. These features (36, 45.7, 46.2, 47.4, 51.6, and 61.9°) produce a reasonable match for diffraction from a $\text{Sc}_6\text{WO}_{12}$ secondary phase (Blasse 1969). $\text{Sc}_6\text{MoO}_{12}$ may also be present, despite the lack of a known diffraction pattern for this compound. We anticipate an inability to resolve diffraction from both tungstenate and molybdate phases given the similar ionic radii of W^{6+} and Mo^{6+} and the isomorphous nature of their other common oxides with Sc. Isomorphous phases would also be conducive to substitution of these cations. Although this analysis does not provide conclusive evidence of tungstenate and molybdate formation, it indicates that secondary phase formation has occurred and suggests that W and Mo are altering the vaporization/condensation reaction.

CONCLUSIONS

We have demonstrated that the surface morphology of ceramic spacers within the interelectrode gap of a converter is altered with vaporization. Alumina shows grain growth with thermal annealing and both terrace development and larger scale grain boundary relief with vaporization. The presence of an oxygen active refractory metal like Ta, either at the surface or in the near-surface vapor phase, can significantly alter the morphology of alumina. The result is to limit the terrace propagation length and produce a morphology with greater degree of vertical structure. Scandia also shows considerable vertical texture development produced by vaporization at grain and void edges, however no morphological impact was observed for Ta. Re-deposition of sublimated material produces large-scale deposit morphology at the scandia surface. Mo and W may play a role in deposit formation, with the possibility of secondary phase formation. The fact that re-deposition occurs on the scandia surface and not the alumina suggests that the condensation reaction mechanism is affected differently for these two materials.

Acknowledgments

This work was funded by the Defense Nuclear Agency. The work was performed at Sandia National Laboratories and supported by the U.S. Department of Energy under Contract No. DE-AC04-94-AL85000.

References

- Baksh, F. G., G. A. Dyuzhev, A. M. Martsinovskiy, B. Ya. Moyzhes, G. Ye. Pikus, E. B. Sonin and V. G. Yur'yev (1978) "Thermionic Converters and Low Temperature Plasma," Technical Information Center/U.S. DOE, DOE-tr-1: 5-8.
- Blasse, G. (1969) "Lanthanide Tellurates $\text{Ln}_6\text{TeO}_{12}$," *J. Inorg. Nucl. Chem.*, 31: 3335-3336.
- Heffelfinger, J.R., M. W. Bench and C. B. Carter (1995) "On the Facetting of Ceramic Surfaces," *Surf. Sci.*, 343: L1161-L1166.
- Hirth, J.P., and G. M. Pound (1957) "Evaporation of Metal Crystals," *J. Chem. Phys.*, 26(5): 1216-1224.
- Kozlov, O. F., V. I. Uvarov and D. L. Tsetskladze (1993) "Corrosion of Aluminum Oxide in the Interelectrode Medium of a Thermionic Converter," *High Temperature Thermal Physics*, 30;2: 400-405.

Kozlov, O. F., Y. V. Nikolaev, V. Vybyvanets, P. Agnew, D. Olson and K. R. Zavadil (1995) "Research of Ceramic Materials Stability in the Thermionic Converter Interelectrode Gap," in *Proc. 12th Symposium on Space Nuclear Power and Propulsion*, CONF-950110, M. S. El-Genk, ed., American Institute of Physics, New York, AIP Conference Proceedings No. 324;1: 271-276.

Lamoreaux, R. H., D. L. Hildenbrand and L. Brewer (1987) "High Temperature Vaporization Behavior of Oxides II," *J. Phys. Chem Ref. Data.*, 16(3): 419-443.

Peleg, M. and C. B. Alcock (1974) "The Mechanism of Vaporization and the Morphological Changes of Single Crystals of Alumina and Magnesia at High Temperatures," *High Temp. Sci.*, 6: 52-63.

Paule, R. C. and J. L. Margrave (1967) "Free Evaporation and Effusion Techniques," in *The Characterization of High Temperature Vapors*, J. L. Margrave, ed., John Wiley and Sons, New York, 130-151.

Roth, R. S. and J. L. Waring (1970) "Effect of Oxide Additions on the Polymorphism of Tantalum Pentoxide," *J. Res. National Bureau of Standards*, 74A: 485-493.